**Timm Weitkamp**

# Imaging and Tomography with High Resolution Using Coherent Hard Synchrotron Radiation

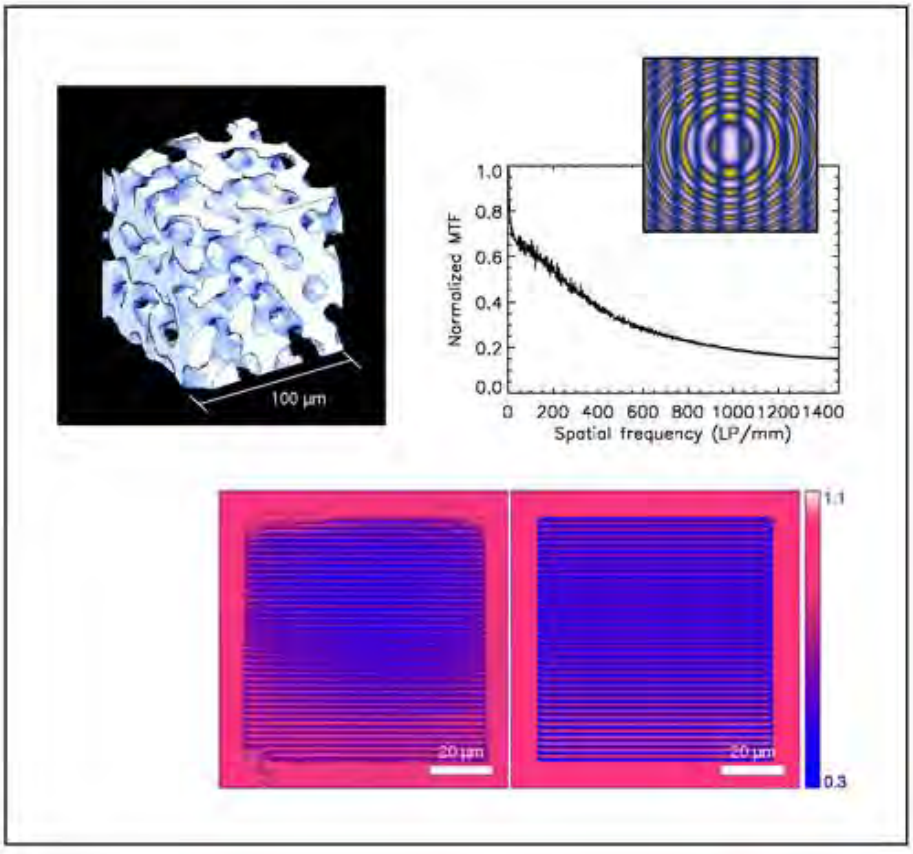


Cuvillier Verlag Göttingen

# Imaging and Tomography with High Resolution Using Coherent Hard Synchrotron Radiation

Dissertation
zur Erlangung des Doktorgrades
des Fachbereiches Physik der Universität Hamburg

vorgelegt von

Timm Weitkamp

aus Malsch

Grenoble
2002

**Bibliografische Information Der Deutschen Bibliothek**
Die Deutsche Bibliothek verzeichnet diese Publikation in der Deutschen Nationalbibliografie; detaillierte bibliografische Daten sind im Internet über http://dnb.ddb.de abrufbar.
1. Aufl. - Göttingen : Cuvillier, 2002
Zugl.: Hamburg, Univ., Diss., 2002
ISBN 3-89873-609-1

| | |
|---|---|
| Gutachter der Dissertation: | Prof. Dr. G. Materlik<br>Prof. Dr. G. Zimmerer |
| Gutachter der Disputation: | Prof. Dr. G. Materlik<br>Prof. Dr. R. L. Johnson |
| Datum der Disputation: | 25. Oktober 2002 |
| Vorsitzender des Prüfungsausschusses: | Dr. K. Petermann |
| Vorsitzender des Promotionsausschusses: | Prof. Dr. F.-W. Büßer |
| Dekan des Fachbereichs Physik: | Prof. Dr. F.-W. Büßer |


Nonnenstieg 8, 37075 Göttingen
Telefon: 0551-54724-0
Telefax: 0551-54724-21
www.cuvillier.de


1. Auflage, 2002
Gedruckt auf säurefreiem Papier

ISBN 3-89873-609-1

# Abstract

The design, characterization, application, and study of possible performance improvement of a high-resolution X-ray microimaging and microtomography instrument at the undulator beamline ID 22 of the European Synchrotron Radiation Facility (ESRF) in Grenoble, France, are reported. The instrument features a spatial resolution of below one micrometer (full width at half maximum of the detector line-spread function: 0.5 μm), detector linearity within less than 2 per cent, fast detector readout (≈ 100 ms) and low noise, and is optimized for the photon energy range between 10 and 30 keV. In addition to absorption contrast conventionally used in radiography, the coherence properties of the third-generation synchrotron-radiation beam give access to in-line phase contrast. Applications of the instrument are demonstrated that make use of its unique performance characteristics with respect to spatial resolution, contrast, and time resolution. Thus, a microtomography study of paper yields information both on the cellulose fiber network and on the structure of individual fibers. Phase contrast gives access to the structure of paper soaked in water, invisible in absorption contrast. In another study, the intense X-ray beam together with the low noise and fast readout of the detector allow time-resolved imaging of non-equilibrium growth processes in solidifying alloys. The studies are qualitatively unprecedented and rely crucially on the instrument characteristics. To further improve the performance of high-resolution X-ray imaging, the potential of using compound refractive lenses (CRLs) is investigated experimentally and by numerical simulations of image formation in Fresnel wave propagation, with computer code especially written for the purpose. X-ray lenses in imaging geometry may be used to obtain sharp images of objects far from the detector, without the degrading effects of Fresnel diffraction and penumbral blurring that occur in conventional radiography. Furthermore, with suitable geometry, the obtained image is magnified. In this way, imaging at spatial resolutions exceeding that of the detector, or hard X-ray microscopy, becomes possible. The experiments show that presently available CRLs, made of aluminum, can be used for beamline diagnostical imaging applications such as imaging of the source or of optical components that are not accessible to direct inspection. In microscopy applications, the first hard X-ray microscopic tomography is reported, demonstrating that the surface quality of the parabolic lenses is high enough to ensure the absence of image distortions. The resolution of the CRL tomograms is slightly better than 1 μm. Substantial further improvements in resolution are somewhat impaired by the absorption profile of the aluminum lenses, which limits the effective numerical aperture of the X-ray microscope and leads to specific phase artifacts in the micrographs. The simulations reproduce these artifacts and show that lenses made of beryllium will reduce if not eliminate the problem, so that CRL microscopy with a resolution of 100 nm can be envisioned.

# Zusammenfassung

Die vorliegende Arbeit behandelt Konstruktion, Charakterisierung und Anwendung eines hochauflösenden Mikroradiographie- und Mikrotomographie-Geräts am Undulatorstrahlrohr ID 22 der Europäischen Synchrotronstrahlungsquelle ESRF in Grenoble (Frankreich) sowie Untersuchungen zur Erweiterung der Leistungsfähigkeit von Gerät und Methode durch Verwendung von Röntgenlinsen. Der Flächendetektor des Instruments hat ein räumliches Auflösungsvermögen unterhalb eines Mikrometers (volle Halbwertsbreite der Linienantwortfunktion 0.5 μm), eine Detektorlinearität besser als 2 Prozent sowie eine schnell auslesende ($\approx$ 100 ms) und rauscharme CCD-Elektronik und ist optimiert für Photonenenergien zwischen 10 und 30 keV. Die Kohärenzeigenschaften der Röntgenstrahlen aus dem ESRF-Undulator ermöglichen die Ausnutzung von Inline-Phasenkontrast, der eine Hervorhebung von Grenz- und Oberflächen in der Probe bewirkt und für zahlreiche schwach absorbierende Systeme um Größenordnungen stärker ist als der üblicherweise ausgenutzte Absorptionskontrast. Anwendungsbeispiele werden präsentiert, in denen die Leistungsmerkmale des Geräts bezüglich räumlicher Auflösung, Kontrast und Zeitauflösung entscheidend sind. So liefern mikrotomographische Messungen an Papier nicht nur dreidimensionale Information über die Struktur des Zellulosefasernetzwerks, sondern auch innere Strukturparameter der Fasern. Die Nutzung von Phasenkontrast ermöglicht derartige Messungen auch an in Wasser eingetauchten Proben, für welche kein meßbarer Absorptionskontrast auftritt. In einem weiteren Experiment erlauben das geringe Rauschen des Detektors und seine schnelle Auslese in Kombination mit der hohen Röntgenflußdichte zeitaufgelöste Bildserien von Nichtgleichgewichts-Wachstumsprozessen bei der Erstarrung von Metallschmelzen. Mit dem Ziel noch besserer Auflösung und Bildqualität werden schließlich Möglichkeiten des Einsatzes modularer refraktiver Röntgenlinsen (engl. *compound refractive lenses*, CRLs) in bildgebender Geometrie untersucht, und zwar sowohl experimentell als auch durch Simulationsrechnungen mit eigens entwickelter Software zur Bildentstehung durch Fresnel-Propagation. Abbildungssysteme mit Röntgenlinsen liefern scharfe Bilder weit vom Detektor entfernter Strukturen ohne Halbschatteneffekte und Fresnelbeugung. Bei geeigneter Geometrie ist das Bild vergrößert. Der Aufbau stellt dann ein einfaches Röntgenmikroskop dar und ermöglicht Radiographie mit einer räumlichen Auflösung, die jene des Detektors übertrifft. Die Experimente zeigen, daß derzeit verfügbare CRLs aus Aluminium nutzbringend für strahldiagnostische Zwecke wie das Abbilden der Röntgenquelle oder von röntgenoptischen Komponenten im Strahlverlauf eingesetzt werden können. Im Bereich der röntgenmikroskopischen Anwendungen ist es gelungen, mikroskopische Tomogramme aufzunehmen. Dies demonstriert unter anderem das verzerrungsfreie Abbildungsverhalten der CRLs. Die Auflösung der CRL-mikroskopischen Tomogramme ist etwas besser als 1 μm. Das Erreichen deutlich höherer Auflösung wird durch das Absorptionsprofil der Aluminiumlinsen erschwert, das die effektive numerische Apertur des Mikroskopobjektivs begrenzt und zu charakteristischen Phasenartefakten in den Bildern führt. Diese werden von Simulationsrechnungen reproduziert. Die Rechnungen zeigen, daß aus Beryllium gefertigte CRLs die störenden Phänomene in so viel schwächerem Ausmaß zeigen, daß sie Auflösungen um 100 nm erlauben werden.

# Contents

# Introduction

Hard X-ray microradiography and microtomography with high resolution gives access to the two- or three-dimensional real-space electron-density structure of opaque materials, with spatial resolution down to the micrometer range at sample thicknesses up to a few millimeters. It is an inherently nondestructive technique and allows a great variety of mechanical, thermodynamical, and chemical sample environments. These characteristics make it complementary to other real-space methods such as confocal laser scanning microscopy, electron microscopy, or neutron radiography, and to reciprocal-space methods such as crystal diffraction and small-angle scattering. Today, high-resolution X-ray microimaging and tomography find applications in such diverse research fields as materials science, metallurgy, environmental chemistry, biochemistry, biomaterials science, and astrophysics [Bon99, Bon02]. Microtomography devices are today available to research and industry in various forms, often based on laboratory tube X-ray sources, where they can resolve structures down to less than 5 μm in size [IJGL02, Sas02].

The use of synchrotron radiation for microimaging including tomography was first proposed and demonstrated in the 1980s. The availability of third-generation synchrotron radiation (SR) sources such as the European Synchrotron Radiation Facility (ESRF) in Grenoble, France, led to substantial qualitative progress in the development of X-ray microimaging in at least two ways: Firstly, the high degree of spatial coherence of the X rays from third-generation SR sources allows in-line phase-contrast imaging. In-line phase contrast is generated in a conventional radiography setup, provided the illumination is partially coherent, through the formation of a Fresnel diffraction image of the sample in the propagation space between sample and detector [SSK$^+$95, CBB$^+$96, WGG$^+$96, Koh98]. For small sample-to-detector distances, it takes the form of an enhancement of edges in the object. Images recorded in this regime can be used directly to extract morphological information and can be tomographically reconstructed [RSS$^+$96, CPSB$^+$97, SRSS99, WRS99, WRS$^+$02]. Another approach is the reconstruction of the phase shift distribution in the object projections, which in the case of tomographic reconstruction yields the distribution of refractive index in the sample. Several methods have been demonstrated or proposed for phase reconstruction from projections taken at one or more sample-to-detector distances [Koh97, PN98, CLB$^+$99, Bro99, GRS$^+$99, GSP$^+$02, SYU02].

Whichever treatment is preferred for phase-contrast images, its major advantage is that for weakly absorbing samples or samples whose different structural regions show similar X-ray absorption, in-line phase contrast is orders of magnitude more sensitive than conventional amplitude contrast. Moreover, the required experimental setup is simple

compared to such other phase-sensitive methods as interferometric phase contrast [BH65, Mom95, BBBG97] or diffraction-enhanced imaging [IB95, CTJ+97].

The second asset of third-generation synchrotron radiation, especially from such sources as wigglers or undulators, is its high flux density. This not only allows tomographic imaging at unprecedented spatial resolution with good signal-to-noise ratio and short data acquisition times in the range of minutes, but also time-resolved radiographic studies at high spatial resolution.

For the exploitation of these potentials opened up by the powerful radiation source, image detectors are needed that combine fast readout, low noise, and a high dynamic range. The most viable and now widely used scheme to meet these criteria is that of a thin single-crystal scintillator screen that converts the X-ray image to visible light, a microscope to magnify the visible-light image, and a CCD camera to detect the magnified image. Using this scheme, the spatial resolution in SR hard X-ray imaging reaches values slightly better than 1 μm [KRSS98, KCL+00, USY+02].

This limit to the spatial resolution of radiography is given by several independent factors, mostly by the resolution of the detector and by FRESNEL diffraction on the object. In imaging objects far away from the position of the detector, the image is further blurred by convolution with the projected source size. One approach to overcome all of these limits is the use of an X-ray lens as objective in a full-field hard X-ray microscope. This approach has been pursued successfully in the soft X-ray domain [Sch93, Jac98]. With hard X rays, it has not been feasible until recently because lenses for the photon energy range above $\approx$ 10 keV were not available. This problem is, however, in the process of being solved. Two categories of hard X-ray lenses have been presented in the past few years that have a potential for hard X-ray imaging. These are, on the one hand, zone plates. While these diffractive devices have been available in high quality for soft X rays for years, the development of hard X-ray zone plates presents a more demanding technological challenge and was only successful in recent years [LYL+92, DRG+99, YLK+99, PSP+99, DNZ01, TYM+02]. At approximately the same time, the feasibility of refractive X-ray lenses was experimentally demonstrated [SKSL96] and triggered the development of many different devices based on this principle [LSR+99, AGK+00, DKK+00, CCD+00a, PBG+01].

The development of full-field hard X-ray microscopy using diffractive or refractive lenses is still in the early stages of its development. Zone-plate microscopy was demonstrated by several groups with promising results and at resolutions of a few hundred nm [LYX+95, LWD+00, KYI+02]. Its development is continuing, reaching resolutions beyond 100 nm [RNSH02]. Microcapillary refractive lenses have been used to obtain a resolution of 800 nm [KOT+01]. Among those hard X-ray micrographs with the best reported overall image quality for X-ray microscopy above 10 keV, taking into account the combination of such quality criteria as field of view, resolution, and absence of distortions, are images obtained with parabolic compound refractive lenses (CRLs) made of aluminum [LSR+99, LST+99, WRS+02, SBG+02b]. These lenses were also used to demonstrate hard X-ray microscopic tomography [RWS+01, SGB+01, WRS+02, SBG+02a, SMK+02]. The

current resolution limits are approximately 500 nm for projection CRL microscopy with small field of view, and 900 nm for CRL microscopic tomography.

The goal of the present work is the development and optimization of a high-resolution microradiography and tomography instrument for absorption and in-line phase contrast imaging at the undulator beamline ID 22 at the ESRF, as well as the further investigation of the potential of CRLs in high-resolution X-ray imaging, including a more detailed study on contrast formation and intrinsic artifacts. Chapters 1 through 4 review the physical and mathematical concepts and computational methods underlying coherent imaging with hard X rays as well as absorption and phase-contrast tomography. Chapter 5 presents the new instrument at ID 22 and its performance characteristics. In chapter 6, exemplary applications of the instrument are presented and discussed. These experiments were carried out in collaboration with researchers from other disciplines and institutes, who had an interest in the method for the investigation of their samples. The examples represent studies that were not possible previously and rely on the outstanding performance characteristics of the instrument with respect to contrast, spatial resolution, low noise, and time resolution.

Chapter 7 addresses imaging with compound refractive lenses. The development of these lenses is the subject of a collaboration between ESRF and the Rheinisch-Westfälische Technische Hochschule (RWTH) in Aachen, Germany, and most of the experiments are carried out together with researchers from RWTH. Experimental and theoretical investigations of image formation in CRL imaging setups are presented. A series of experiments on different beamlines show the use of CRLs in beamline-diagnostic imaging. As for magnified imaging with optimized spatial resolution, simulation calculations as well as experimental studies are carried out that show the limiting factors for spatial resolution with current CRL setups, and how these can be overcome with beryllium as a new lens material. The first experimental realization of tomography with a hard X-ray microscope is reported.

# Chapter 1

# Interaction of X Rays with Matter

In hard X-ray transmission imaging, a beam of electromagnetic radiation with wavelengths in the range between approximately 0.2 and 2 Å, corresponding to photon energies between 6 and 60 keV, i. e., a *hard X-ray* beam, traverses an object under study, and the intensity distribution in a plane normal to the beam propagation direction somewhere downstream of the object is measured with a two-dimensional position-sensitive detector (figure 1.1). This intensity distribution, or *image*, is determined by the interaction of the X rays with the sample material. In this chapter we will briefly discuss the interaction processes that are important in hard X-ray imaging.

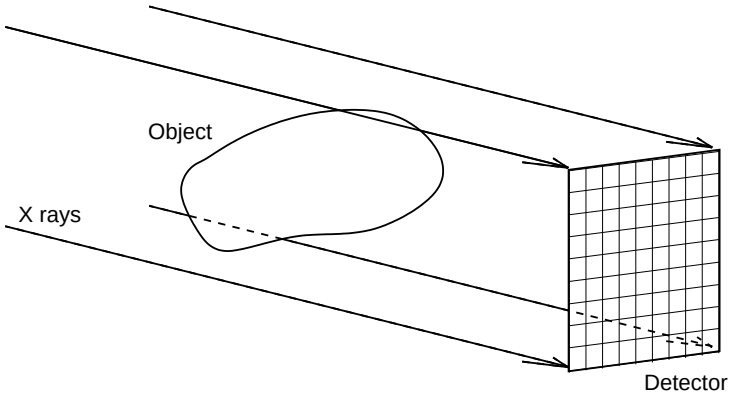


**Figure 1.1:** Principle of hard X-ray transmission imaging.

The main processes by which X rays interact with matter are photoelectric absorption and elastic as well as inelastic scattering of X rays by electrons.[1] Multiple elastic scattering in the forward direction, which occurs in all materials regardless of their atomic ordering, is coherent because it does not change the wavelength of the radiation nor the phase relation between parts of the wave scattered on scatterers at different locations. It gives rise to such macroscopic phenomena as refraction and surface reflection. Scattering, elastic or

[1] Scattering by atomic nuclei or by collective excitations in crystalline solids (phonons, magnons and other quasi-particles) will be neglected. So will electron-positron pair production, which occurs only at photon energies above 1 MeV.

inelastic, into other directions will be regarded only as a contribution to the attenuation of the forward beam or as noise.

## 1.1 Forced Damped Oscillator Model

A relatively simple model that we will use to introduce the concept of a complex refractive index and the phenomenon of anomalous dispersion is that of the atomic electrons seen as classical oscillators, with the natural frequency of each oscillator representing an atomic absorption frequency. This treatment goes back to COMPTON, who adapted the theory developed earlier for the visible wavelength region by LORENTZ. We follow JAMES [Jam82] in the presentation of the fundamental results.

We describe an atomic electron as a classical oscillator of natural angular frequency $\omega_q$ (where $q$ denotes the orbital shell, and $\omega_q$ corresponds to the absorption resonance) under a restoring force $-m\omega_q^2 x$, i. e., a harmonic oscillator ($m$: mass of the electron; $x$: displacement). The oscillation is damped because an accelerated charged particle radiates energy. The damping factor $\gamma$ can be derived from classical electrodynamics. Let the electron further be in a linearly polarized external plane wavefield, $E(z,t) = E_0 \exp(\mathrm{i}\omega(z/c - t))$. Figure 1.2 illustrates the model. The equation of motion for the electron is

$$\ddot{x} + \gamma\dot{x} + \omega_q^2 x = -\frac{e}{m} E_0 \mathrm{e}^{\mathrm{i}\omega(z/c-t)} , \tag{1.1}$$

Solutions of equation 1.1 are of the form

$$x(t) = -\frac{e}{m}\frac{1}{(\omega_q^2 - \omega^2) - \mathrm{i}\gamma\omega} E(z,t) . \tag{1.2}$$

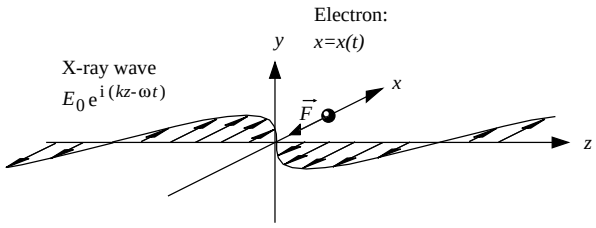


**Figure 1.2:** Illustration of the LORENTZ model.

The displacement $x(z,t)$ of the electrons of type $q$ leads to a polarization

$$P_q = -n_q e x . \tag{1.3}$$

The contribution of electrons of this type to the dielectric susceptibility, $\chi_q$, is then

$$\chi_q = \frac{P_q}{\epsilon_0 E} \qquad \text{(definition of the dielectric susceptibility)} \tag{1.4}$$

$$= -\frac{n_q e^2}{\epsilon_0 m} \frac{1}{\omega_q^2 - \omega^2 - \mathrm{i}\gamma\omega} \qquad \text{(substituting eq. 1.2 into eq. 1.3)} . \tag{1.5}$$

Separating the real and imaginary parts, we get

$$\chi_q = -2\delta_q + \mathrm{i}2\beta_q \,, \tag{1.6}$$

$$\delta_q = \frac{n_q e^2}{2\epsilon_0 m} \frac{\omega^2 - \omega_q^2}{(\omega^2 - \omega_q^2)^2 + \gamma^2\omega^2} \,, \tag{1.7}$$

$$\beta_q = \frac{n_q e^2}{2\epsilon_0 m} \frac{\gamma\omega}{(\omega^2 - \omega_q^2)^2 + \gamma^2\omega^2} \,. \tag{1.8}$$

Figure 1.3 shows $\delta_q$ and $\beta_q$ as the oscillator model predicts them around the resonance frequency $\omega_q$. The strong variation of the dielectric susceptibility near resonance frequencies is called *anomalous dispersion*.

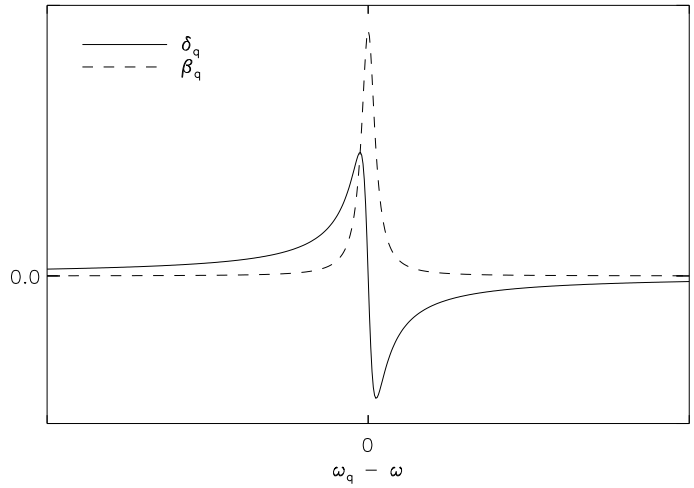


**Figure 1.3:** At the resonance frequency $\omega_q$ of atomic electrons in shell $q$, the oscillator model predicts a peak in $\beta_q$ and sign reversal of $\delta_q$. These strong fluctuations of the real and imaginary part of the dielectric susceptibility near a resonance frequency are called anomalous dispersion.

## 1.2 Complex Refractive Index

The refractive index is defined as the ratio of the phase velocities in vacuum, $c$, and in the medium, $v_q$. For a medium consisting of $q$-type electrons, it is

$$\frac{c}{v_q} = \sqrt{1 + \chi_q} \approx 1 - \delta_q + \mathrm{i}\beta_q \,, \tag{1.9}$$

where we have used the fact that both $\delta_q$ and $\beta_q$ are much less than unity for X-ray wavelengths.

The phase velocity is thus complex. The resultant wave in the medium,

$$E_q(z,t) = E_{0,q}\,\mathrm{e}^{\mathrm{i}\omega(\frac{1}{v_q}z-t)} \tag{1.10}$$

$$= E_{0,q}\,\mathrm{e}^{-k\beta_q z}\,\mathrm{e}^{\mathrm{i}k(1-\delta_q)z}\,\mathrm{e}^{-\mathrm{i}\omega t}\,; \quad k=\frac{\omega}{c}=\frac{2\pi}{\lambda}\,, \tag{1.11}$$

is both attenuated in amplitude and shifted in phase, and the real and imaginary parts of the refractive index respectively describe phase shift and attenuation.

In a real case, where the medium has electrons in different orbital shells and possibly different sorts of atoms, the contributions of all types of electrons $q$ to the dielectric susceptibility $\chi$ add up, and so do the contributions to $\delta$ and $\beta$, the real and imaginary parts of the complex refractive index. The resulting complex refractive index for a real medium is therefore

$$n = 1-\sum_q \delta_q + \mathrm{i}\sum_q \beta_q = 1-\delta+\mathrm{i}\beta\,. \tag{1.12}$$

## 1.3 Refraction

The quantity $\delta$ is called the decrement of the refractive index. It describes the phase shift of the forward-propagating wave and thus, together with the geometry of the object, the refraction of radiation that passes through a material.

Despite the simplicity of the oscillator model, equation 1.7 leads to a quantitatively correct expression for $\delta$ in the limit of short wavelengths, i. e., at photon energies far above all absorption edges of the material, where $\omega \gg \omega_q$ for all $q$. In this region we can approximate $\omega^2-\omega_q^2 \approx \omega^2$ and, neglecting the damping term in the denominator, we can write,

$$\delta = \sum_q \delta_q \tag{1.13}$$

$$= \frac{e^2}{2\epsilon_0 m}\sum_q \frac{n_q}{\omega^2-\omega_q^2} \tag{1.14}$$

$$\approx \frac{e^2}{2\epsilon_0 m}\frac{1}{\omega^2}\underbrace{\sum_q n_q}_{n_\mathrm{e}}\,, \tag{1.15}$$

where $n_\mathrm{e}$ is the electron number density in the material,

$$n_\mathrm{e} = \frac{N_\mathrm{A} Z\rho}{A}\,. \tag{1.16}$$

Here, $N_\mathrm{A}$ is Avogadro's number, $A$ the atomic weight, $Z$ the atomic number, and $\rho$ the density of the material. Using the photon energy $E_\gamma = \hbar\omega$, we get

$$\delta = \underbrace{\frac{N_\mathrm{A}\hbar^2 e^2}{2\epsilon_0 m}}_{4.15\times10^{-4}\ \mathrm{keV^2\,cm^3\,mol^{-1}}}\frac{1}{E_\gamma^2}\frac{Z\rho}{A}\,. \tag{1.17}$$